Suppression of backscattered diffraction from sub-wavelength 'moth-eye' arrays

Petros I. Stavroulakis,[1,*] Stuart A. Boden,[1] Thomas Johnson,[1] and Darren M. Bagnall[1]

[1]*Nano Research Group, Electronics and Computer Science, University of Southampton, University Road, Southampton, Hampshire SO17 1BJ, UK*

[*]*pjs05r@ecs.soton .ac.uk*

Abstract: The eyes and wings of some species of moth are covered with arrays of nanoscale features that dramatically reduce reflection of light. There have been multiple examples where this approach has been adapted for use in antireflection and antiglare technologies with the fabrication of artificial moth-eye surfaces. In this work, the suppression of iridescence caused by the diffraction of light from such artificial regular moth-eye arrays at high angles of incidence is achieved with the use of a new tiled domain design, inspired by the arrangement of features on natural moth-eye surfaces. This bio-mimetic pillar architecture contains high optical rotational symmetry and can achieve high levels of diffraction order power reduction. For example, a tiled design fabricated in silicon and consisting of domains with 9 different orientations of the traditional hexagonal array exhibited a ~96% reduction in the intensity of the −1 diffraction order. It is suggested natural moth-eye surfaces have evolved a tiled domain structure as it confers efficient antireflection whilst avoiding problems with high angle diffraction. This combination of antireflection and stealth properties increases chances of survival by reducing the risk of the insect being spotted by a predator. Furthermore, the tiled domain design could lead to more effective artificial moth-eye arrays for antiglare and stealth applications.

OCIS codes: (050.0050) Diffraction and gratings; (050.6624) Subwavelength structures.

References and links

1. C. G. Bernard, "Structural and functional adaptation in a visual system," Endeavour **26**, 79–84 (1967).
2. P. R. Stoddart, P. J. Cadusch, T. M. Boyce, R. M. Erasmus, and J. D. Comins, "Optical properties of chitin: surface-enhanced Raman scattering substrates based on antireflection structures on cicada wings," Nanotechnology **17**(3), 680–686 (2006).
3. A. Yoshida, M. Motoyama, A. Kosaku, and K. Miyamoto, "Antireflective nanoprotuberance array in the transparent wing of a hawkmoth, Cephonodes hylas," Zoolog. Sci. **14**(5), 737–741 (1997).
4. D. G. Stavenga, S. Foletti, G. Palasantzas, and K. Arikawa, "Light on the moth-eye corneal nipple array of butterflies," Philos. Trans. R. Soc. London, Ser. B **273**(1587), 661–667 (2006).
5. S. J. Wilson and M. C. Hutley, "The optical properties of "moth eye" antireflection surfaces," J. Mod. Opt. **29**, 993–1009 (1982).
6. P. Clapham and M. C. Hutley, "Reduction of lens reflexion by the "moth eye" principle," Nature **244**(5414), 281–282 (1973).
7. A. Gombert, K. Rose, A. Heinzel, W. Horbelt, C. Zanke, B. Bläsi, and V. Wittwer, "Antireflective submicrometer surface-relief gratings for solar applications," Sol. Energy Mater. Sol. Cells **54**(1-4), 333–342 (1998).
8. Y. Ono, Y. Kimura, Y. Ohta, and N. Nishida, "Antireflection effect in ultrahigh spatial-frequency holographic relief gratings," Appl. Opt. **26**(6), 1142–1146 (1987).
9. S. J. Wilson and M. C. Hutley, "The optical properties of "moth eye" antireflection surfaces," Opt. Acta (Lond.) **29**(7), 993–1009 (1982).
10. R. C. Enger and S. K. Case, "Optical elements with ultrahigh spatial-frequency surface corrugations," Appl. Opt. **22**(20), 3220–3228 (1983).
11. K. M. Baker, "Highly corrected close-packed microlens arrays and moth-eye structuring on curved surfaces," Appl. Opt. **38**(2), 352–356 (1999).
12. K. Kintaka, J. Nishii, A. Mizutani, H. Kikuta, and H. Nakano, "Antireflection microstructures fabricated upon fluorine-doped SiO(2) films," Opt. Lett. **26**(21), 1642–1644 (2001).

#172279 - $15.00 USD Received 12 Jul 2012; accepted 15 Sep 2012; published 2 Jan 2013

13. H. Toyota, K. Takahara, M. Okano, T. Yotsuya, and H. Kikuta, "Fabrication of microcone array for antireflection structured surface using metal dotted pattern," Jpn. J. Appl. Phys. **40**(Part 2, No. 7B), L747–L749 (2001).
14. J. Nishii, K. Kintaka, Y. Kawamoto, A. Mizutani, and H. Kikuta, "Two dimensional antireflection microstructure on silica glass," J. Ceram. Soc. Jpn. **111**(1289), 24–27 (2003).
15. L. Escoubas, J. J. Simon, M. Loli, G. Berginc, F. Flory, and H. Giovannini, "An antireflective silicon grating working in the resonance domain for the near infrared spectral region," Opt. Commun. **226**(1-6), 81–88 (2003).
16. M. E. Motamedi, W. H. Southwell, and W. J. Gunning, "Antireflection surfaces in silicon using binary optics technology," Appl. Opt. **31**(22), 4371–4376 (1992).
17. Y. Kanamori, M. Sasaki, and K. Hane, "Broadband antireflection gratings fabricated upon silicon substrates," Opt. Lett. **24**(20), 1422–1424 (1999).
18. P. Lalanne and G. M. Morris, "Antireflection behaviour of silicon subwavelength periodic structures for visible light," Nanotechnology **8**(2), 53–56 (1997).
19. D. L. Brundrett, T. K. Gaylord, and E. N. Glytsis, "Polarizing mirror/absorber for visible wavelengths based on a silicon subwavelength grating: design and fabrication," Appl. Opt. **37**(13), 2534–2541 (1998).
20. Y. Kanamori, K. Hane, H. Sai, and H. Yugami, "100 nm period silicon antireflection structures fabricated using a porous alumina membrane mask," Appl. Phys. Lett. **78**(2), 142–143 (2001).
21. K. Hadobás, S. Kirsch, A. Carl, M. Acet, and E. F. Wassermann, "Reflection properties of nanostructure-arrayed silicon surfaces," Nanotechnology **11**(3), 161–164 (2000).
22. S. A. Boden and D. M. Bagnall, "Bio-mimetic subwavelength surfaces for near-zero reflection sunrise to sunset," in *Proceedings of the 4th IEEE World Conference on Photovoltaic Energy Conversion*, 1358–1361 (2006)
23. H. Sai, H. Fujii, Y. Kanamori, K. Arafune, Y. Ohshita, H. Yugami, and M. Yamaguchi, "Numerical analysis and demonstration of submicron antireflective textures for crystalline silicon solar cells," in *Proceedings of the 4th IEEE World Conference on Photovoltaic Energy Conversion*, **1**, 1191–1194 (2006)
24. V. Boerner, V. Kübler, B. Bläsi, and A. Gombert, "P-20: Antireflection systems for flat panel displays - an overview," SID Symposium Digest of Technical Papers **35**, 306–309 (2004).
25. S. A. Boden and D. M. Bagnall, "Tunable reflection minima of nanostructured antireflective surfaces," Appl. Phys. Lett. **93**(13), 133108 (2008).
26. X. Chen, Z.-C. Fan, J. Zhang, G.-F. Song, and L.-H. Chen, "Pseudo-rhombus-shaped subwavelength crossed gratings of GaAs for broadband antireflection," Chin. Phys. Lett. **27**(12), 124210 (2010).
27. S. A. Boden and D. M. Bagnall, "Nanostructured biomimetic moth-eye arrays in silicon by nanoimprint lithography," Proc. SPIE **7401**, 74010J, 74010J-12 (2009).
28. A. T. D. Bennett and I. C. Cuthill, "Ultraviolet vision in birds: what is its function?" Vision Res. **34**(11), 1471–1478 (1994).
29. A. M. Hynes, H. Ashraf, J. K. Bhardwaj, J. Hopkins, I. Johnston, and J. N. Shepherd, "Recent advances in silicon etching for MEMS using the ASE (TM) process," Sens. Actuators, A **74**(1-3), 13–17 (1999).
30. M. Senechal, *Quasicrystals and Geometry* (Cambridge University Press, 1996).
31. G. J. Parker, M. D. B. Charlton, M. E. Zoorob, J. J. Baumberg, M. C. Netti, and T. Lee, "Highly engineered mesoporous structures for optical processing," Philos. Trans. R. Soc. London, Ser. A **364**, 189–199 (2006).
32. A. Gombert, B. Bläsi, C. Bühler, P. Nitz, J. Mick, W. Hoßfeld, and M. Niggemann, "Some application cases and related manufacturing techniques for optically functional microstructures on large areas," Opt. Eng. **43**(11), 2525–2533 (2004).
33. P. I. Stavroulakis, N. Christou, and D. Bagnall, "Improved deposition of large scale ordered nanosphere monolayers via liquid surface self-assembly," Mater. Sci. Eng. B **165**(3), 186–189 (2009).
34. W.-L. Min, B. Jiang, and P. Jiang, "Bioinspired self-cleaning antireflection coatings," Adv. Mater. (Deerfield Beach Fla.) **20**(20), 3914–3918 (2008).
35. C. H. Sun, P. Jiang, and B. Jiang, "Broadband moth-eye antireflection coatings on silicon," Appl. Phys. Lett. **92**(6), 061112 (2008).
36. M. E. Kiziroglou, X. Li, D. C. Gonzalez, C. H. De Groot, A. A. Zhukov, P. A. J. de Groot, and P. N. Bartlett, "Orientation and symmetry control of inverse sphere magnetic nanoarrays by guided self-assembly," J. Appl. Phys. **100**(11), 113720 (2006).

1. Introduction

The discovery of the antireflection properties of moth corneal surfaces by Bernard [1] in 1967 paved the way for using sub-wavelength texturing for reducing the Fresnel reflection of electromagnetic waves at an abrupt optical interface. Such surfaces, consisting of arrays of closely packed subwavelength pillars, have since been found on the transparent wings of cicada [2] and hawkmoths [3] (Fig. 1) and on the cornea of butterflies [4].

The principle by which these antireflection (AR) surfaces operate is to use a collection of closely packed sub-wavelength pillar features to create the equivalent of a graded refractive index layer. If this layer is deeper than half of the wavelength of the incident light, then the reflectance from the interface is greatly reduced [5]. The main advantage of using such a design instead of a thin-film antireflection layer is that any effective refractive index profile

#172279 - $15.00 USD Received 12 Jul 2012; accepted 15 Sep 2012; published 2 Jan 2013

can be created between the refractive index values of the two media by careful choice of the pillar feature shape. If the pillars are tapered, the fraction of material varies from zero at the tips of the pillars to one at the pillar base, resulting in a gradual change of refractive index across the interface. This effectively smoothes the transition across the interface between two media and therefore ensures that incident light does not encounter a sudden change in refractive index which would cause a large proportion to be reflected. Hence, a high performance graded-index interface which operates well over broad ranges of angles of incidence and wavelengths can be realized.

Another advantage of this technology is that no new materials need to be applied to the surface. This allows for use of the technology on a much larger range of materials compared to thin films and eliminates the issues related with film-substrate adhesion.

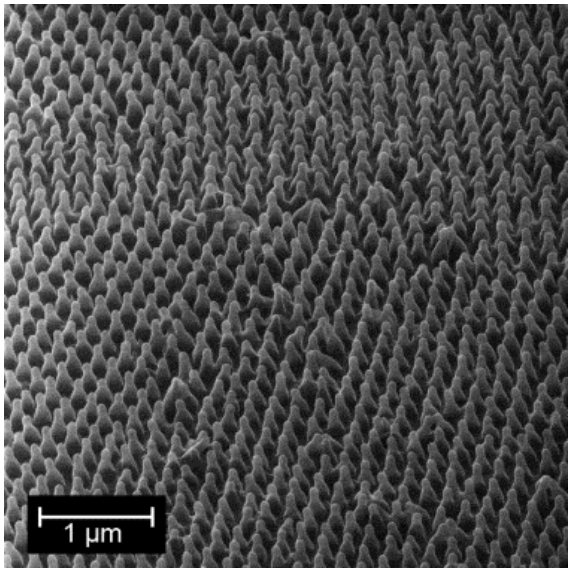

Fig. 1. Helium ion microscope image of nanoscale pillar arrays on the surface of transparent sections of the wings of Cephanodes hylas (sample tilted by 45 degrees)

The very low levels of reflectance achieved by nature using moth-eye arrays have inspired many attempts to replicate such structures in technologically-important materials including photoresist on glass [6–9], in quartz [10–14] and in silicon [15–21]. Applications include solar cells [7,22,23], anti-glare surfaces [24] and stealth technologies [15]. Nanomanufacturing techniques such as e-beam lithography [25], interference/holographic lithography [26] and nano-imprint lithography [27] are often employed for this, however these processes lend themselves to the formation of regular arrays of pillars arranged in a square or hexagonal array across the whole of the patterned area. On the contrary, this is not what is found in natural moth-eye arrays, where the structures tend to be arranged in domains, like two-dimensional versions of grains in a polycrystalline solid, within which hexagonal ordering exists, but at different orientations with respect to adjacent domains (Fig. 1). In this work, it is demonstrated that the consequence of using large scale regular domains is the appearance of intense diffraction orders under particular illumination conditions. Whilst much effort has been focused on designing artificial moth-eye arrays with minimal reflectance at normal incidence, the diffractive properties of these large scale periodic arrays have yet to be explored. The implications of this for stealth applications are investigated and a method of minimizing this effect, taking inspiration from the domain structures found in natural moth-eyes, is presented and applied to an e-beam lithography-based fabrication process.

#172279 - $15.00 USD Received 12 Jul 2012; accepted 15 Sep 2012; published 2 Jan 2013

2. Theory

2.1 Diffraction gratings

Large areas of ordered subwavelength-scale features with periods, d, smaller than the wavelength of incident light, λ, behave as diffraction gratings. This means that at normal incidence, the grating period is sufficiently small (d< λ) to suppress all but the zero order in reflection. However, for larger angles of incidence, higher diffraction orders can emerge, as predicted by the grating equation. This is obtained by considering interference between waves reflected from points spaced a distance d (the grating period) apart and is given by [23]:

$$\sin\theta_m - \sin\theta_i = \frac{m\lambda}{d} \tag{1}$$

Where θ_m is the angle measured from the surface normal at which the diffracted beam of order m emerges and θ_i is the angle of incidence also measured from the surface normal. By considering the last order to disappear as d is decreased (m = −1), it can be shown that to ensure no diffraction over all angles of incidence, the grating period must satisfy the condition:

$$d < \frac{\lambda}{2} \tag{2}$$

This analysis has been carried out using the one-dimensional grating equation but it can be applied to 2D gratings such as those formed by regular arrays of pillars in artificial moth-eyes by considering light incident at specific azimuthal angles related to the symmetry of the array. By drawing lines connecting nearest neighbour pillars with a spacing s, planes can be identified that form a diffraction grating for light incident perpendicular to them (Fig. 2(a)). The grating period, d, is now the inter-plane spacing and for a hexagonal array, is given by:

$$d = \frac{\sqrt{3}}{2}s \tag{3}$$

The gratings formed by the planes of pillars diffract light into orders and angles described by the grating equation (Eq. (1)). For sufficiently small pillar periods (~200-400nm) such as the ones normally used for the design of 'moth-eye' antireflection surfaces in the visible spectrum, only the −1 diffraction order appears at high angles of incidence. Taking a hexagonal array of pillars with a periodicity of 250 nm and using Eq. (1) with m = −1, the wavelength can be plotted as a function of diffracted angle and angle of incidence, mapping out the parameter space in which the −1 order exists (Fig. 2(b) and 2(c)). This simple treatment predicts that when illuminated at specific high angles of incidence, a diffraction order with light in the visible spectrum can emerge from a regular artificial moth-eye array. If viewing at the correct angle, this would manifest as intense glare emanating from the illuminated sample, which would cause problems for stealth and display applications.

#172279 - $15.00 USD Received 12 Jul 2012; accepted 15 Sep 2012; published 2 Jan 2013

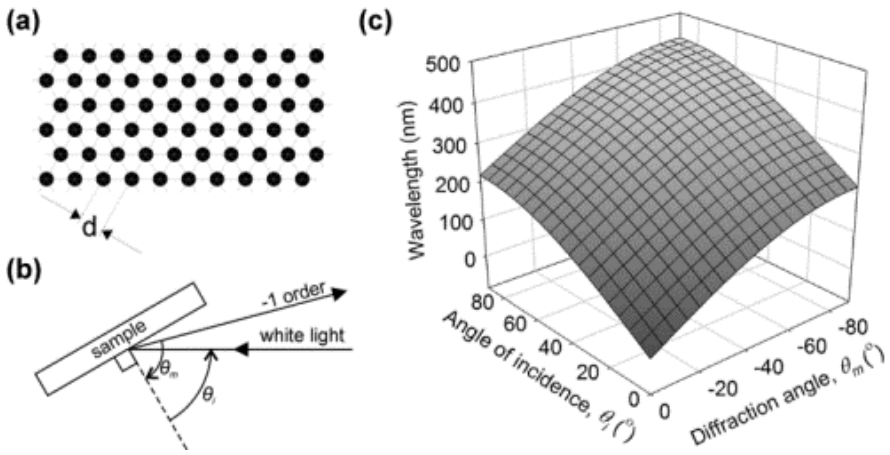

Fig. 2. (a) Diagram of the hexagonal arrangement of pillars viewed from above, showing diffraction planes for specific azimuth angles; (b) diagram viewing in the plane of the sample and showing the incident and diffracted light at an azimuth angle for which the light is incident perpendicular to one of the close packed directions; (c) Plot showing the angle and wavelength parameter space, based on the one-dimensional grating equation, in which the −1 diffraction order exists for a hexagonally arranged moth-eye array with an inter-pillar spacing, *s*, of 250 nm ($d = 216.5$ nm), illuminated with white light.

The grating equation (Eq. (2)) suggests one way to eliminate this effect: The periodicity of the array can be reduced so that Eq. (2) is satisfied for all visible light. However, the pillar height is still required to be at least half of the wavelength for effective antireflection and therefore high aspect ratio features would be required. In addition, the smaller the period, the greater the number of features within an array of a given area, and therefore the more time and expense involved in the manufacture of the structure. Revisiting natural moth eyes, however, suggests an alternative method of reducing the effect of iridescence in subwavelength arrays. If natural moth-eyes consisted of regular arrays of pillars, then they would be ineffective as camouflage because the oblique angle diffraction described above would lead to noticeable iridescence, potentially betraying the location of the animal employing the moth-eye surface to a predator flying past. This would be a particular problem to moths because some of their natural predators, i.e. birds, can have tetrachromatic colour vision and so can see into the near UV [28]. When closely observing the natural moth eye, one notices that the positioning of features is a hybrid arrangement of a close packed pattern in a randomized grid of multi-oriented domains. By breaking the long-range order in this way, diffractive orders are distributed evenly over the azimuthal angle range, reducing the intensity of the diffractive order observed from any particular direction. This effect can be further analysed using Fourier transforms.

2.2 Fourier transform analysis

The generation of a Fourier transform can be used to reveal regularity and periodicity within an image. When performed on top-down images of moth-eye arrays, details of the directional nature of the periodicity can be extracted by observing peaks in the Fourier spectrum. Peaks in the Fourier spectrum will correspond to directions along which strong periodicity exists, and so azimuth angles at which the minus 1 diffraction order will appear. The helium ion microscope was used to image moth-eye structures on the surface of transparent sections of the wings of *Cephanodes hylas* at a range of magnifications (Fig. 3). A fast Fourier transform method (FFT) was then used to generate Fourier spectra of the images, demonstrating a progression of symmetry from six-fold to that of an almost isotropic pattern. The reason for this effect is the inclusion of neighbouring domains with different orientations of the basic close-packed pattern as the magnification of the image is reduced. This creates an increase in optical symmetry because the symmetries of all the different orientations are taken into

#172279 - $15.00 USD Received 12 Jul 2012; accepted 15 Sep 2012; published 2 Jan 2013

account. To confirm this, a collection of tiled patterns was created with the unit cell orientation combinations shown in Fig. 4. Their optical symmetry was then analyzed by taking their 2D Fourier transform (Fig. 4). It was found that by controlling the amount of non-repeating original orientations of the pattern, one can tune the macro-scale rotational optical symmetry of the surface to any integer multiple of the base pattern. However, if an orientation is repeated at an angle that is larger or equal to the base pattern symmetry angle (in this case 60 degrees) it will not contribute to the enhancement of the optical symmetry. This is evident from comparing Fig. 4(a) and 4(f), the addition of the 60 degree orientation has no effect on the number of peaks in the Fourier transform because the peaks are in the same positions as those from the non-rotated pattern.

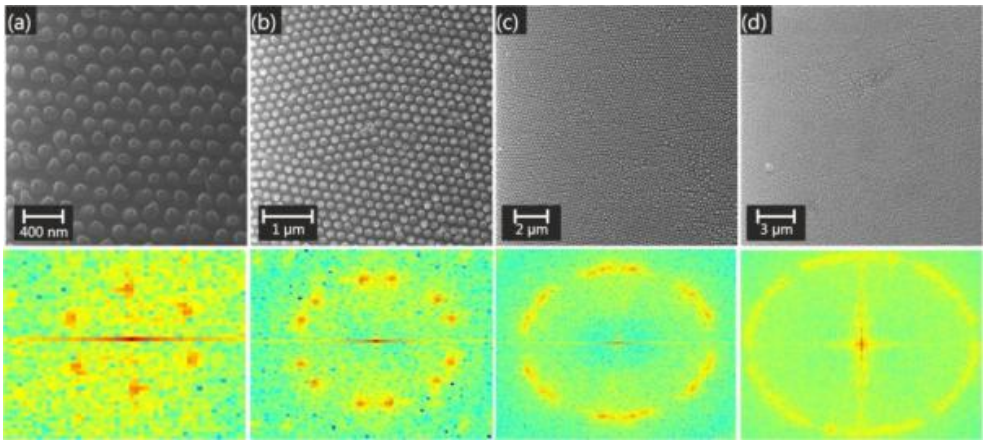

Fig. 3. Helium ion microscope images of moth-eye structures on the surface of transparent wing sections of *Cephanodes hylas*, taken over a range of magnifications. Corresponding Fourier spectra are included below each image.

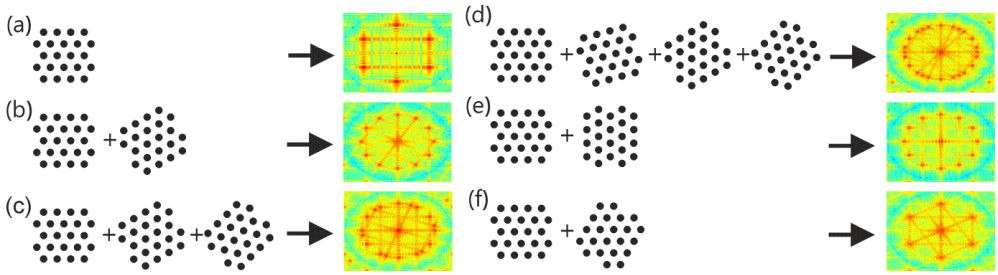

Fig. 4. Fourier transforms of different combinations of the hexagonal close packed pattern at various orientations: a) only 0 degrees b) 0 and 30 degrees c) 0,30 and 45 degrees d) 0, 15, 30 and 45 degrees e) 0 and 90 degrees f) 0 and 60 degrees.

Hence, the order of symmetry of the resulting pattern is found to be the product of the order of the underlying pattern and the number of original orientations one selects to incorporate. The Fourier analysis shows that the formation of differently-orientated domains leads to the distribution of the minus 1 diffraction order across more azimuthal angles. Furthermore, each instance of the diffraction order is decreased in intensity due to the reduced area of the array contributing at any particular angle. To verify this experimentally, artificial moth-eye arrays of various designs were fabricated in silicon and then characterized using a goniometer-type angular reflectance measurement apparatus.

3. Fabrication

Silicon moth-eye samples were fabricated using an e-beam lithography process developed at NILT Technology Ltd. To create the stamp, a 4-inch silicon wafer was first cleaned in fuming

#172279 - $15.00 USD Received 12 Jul 2012; accepted 15 Sep 2012; published 2 Jan 2013

nitric acid and then a 105 nm thick layer of ZEP 520 resist was deposited by spin-coating. A series of patterns consisting of 131 nm diameter disks, with a spacing of 250 nm were defined in the resist layer by e-beam lithography. The resist was developed, forming a mask of holes to be used in a lift-off procedure. Aluminium was deposited to a thickness of 15 nm and then lift-off was performed by placing the wafer into resist stripper at 80°C and sonicating for 10 minutes. This left behind an array of aluminium disks on the wafer in the desired pattern which could then act as an etch mask. An SF_6/C_4F_8 dry etch using the Bosch process (STS Advanced Silicon Etcher MESC Multiplex ICP) was then performed to form vertical pillar walls with a depth of 400nm [29]. Finally, a wet aluminium etch was used to remove the residual aluminium etch mask.

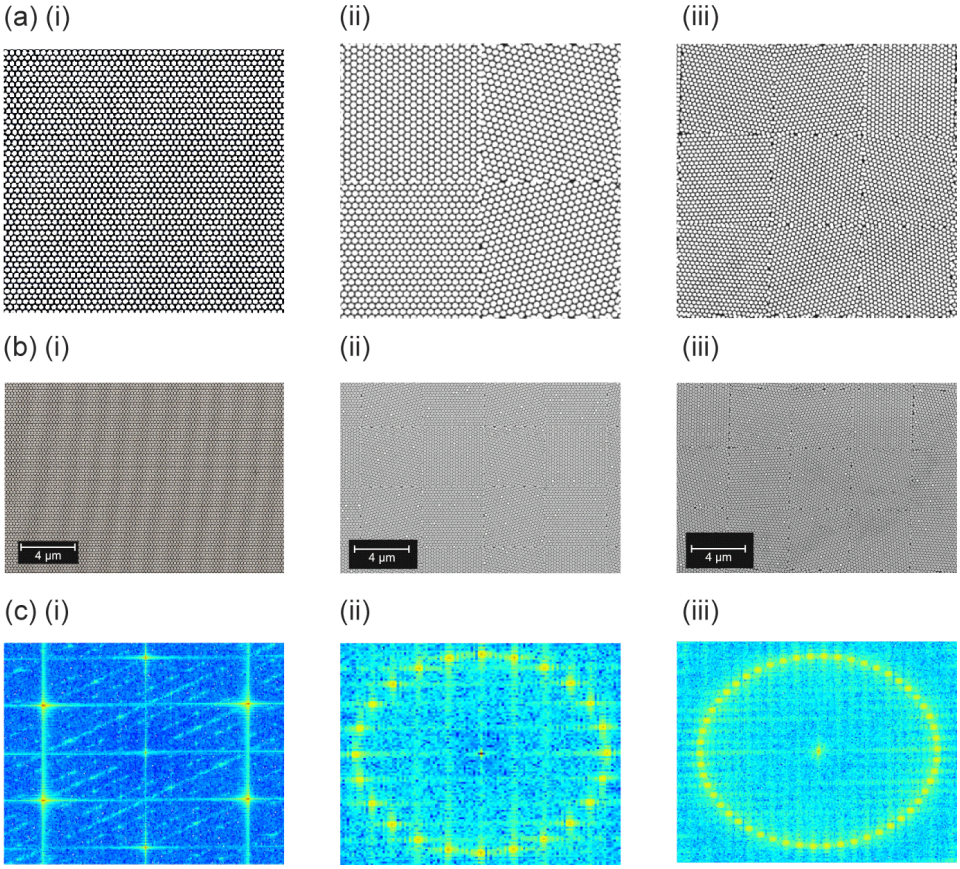

Fig. 5. (a) Unit cells, (b) SEM Images and (c) FFTs of SEM images of moth-eye samples on silicon fabricated in 3 designs based on a hexagonal array: (i) single orientation, (ii) tiled domains with 4 orientations, (iii) tiled domains with 9 orientations.

Three patterns were fabricated in this way, covering an area of 1.4 mm × 1.4 mm. One pattern consisted of a hexagonal, single orientation array. The other two patterns consisted of tiled domains of the hexagonal array used in the first pattern, one with 4 different orientations and the other with 9 different orientations. The unit cells of each pattern are shown in Fig. 5 (a). The number of orientations was chosen to simplify the tiling procedure, since 4 and 9 orientations can be evenly allocated on a square unit cell and tiled so that no two orientations overlap in more than one contingent domain. Since the base symmetry of the hexagonal pattern is 6-fold, using 4 and 9 original orientations results in patterns with an effective 24-fold and 54-fold optical symmetry. The focus of this study was not to minimize the specular reflectance from the sample but to study the intensity of the backscattered diffraction orders,

#172279 - $15.00 USD
Received 12 Jul 2012; accepted 15 Sep 2012; published 2 Jan 2013

thus the pillars were not optimized in shape for antireflection and were made vertical in profile in order to allow for easy detection and measurement of the diffracted orders.

4. Experimental procedure

To fully characterize the backscattered diffraction of the samples, the apparatus shown in Fig. 6 was used. The samples were mounted vertically on rotation stage 3 and then illuminated using a focused beam from a Xenon light source (PVE300, Bentham). A collector fibre optic was mounted on an arm fitted to rotation stage 2 to allow variation in the angle at which light was collected. This was connected to a spectrometer (USB2000, Ocean Optics) to enable spectral analysis of the diffracted light. The angle of incidence and azimuth could be varied independently with use of rotation stage 1 and stage 3 respectively. At certain azimuth angles, an intense strip of light was observed on the fibre optic detector within which there was spectral spreading in the horizontal plane. This intense strip of diffracted light originated from the −1 diffracted order, as predicted theoretically.

Measurements of intensity as a function of azimuth angle were carried out by fixing the angle of incidence θ_i and the angle of detection θ_m and rotating the azimuth angle through 360 degrees whilst monitoring the power of the predicted −1 order wavelength on the fibre optic detector which was recorded by the spectrometer. This was repeated for all samples (Fig. 7(a)).

Additionally, to analyse the spectral spread of the diffraction plane for the single orientation sample, rotation stage 3 was rotated to orientate the sample so that the diffraction order plane was aligned to the horizontal fibre optic detector plane. The collector fibre optic, linked to the spectrometer, was then scanned over the range of diffracted angles, θ_m, to record the wavelength of diffracted light at each diffracted angle. This was repeated for various angles of incidence (Fig. 7(b)).

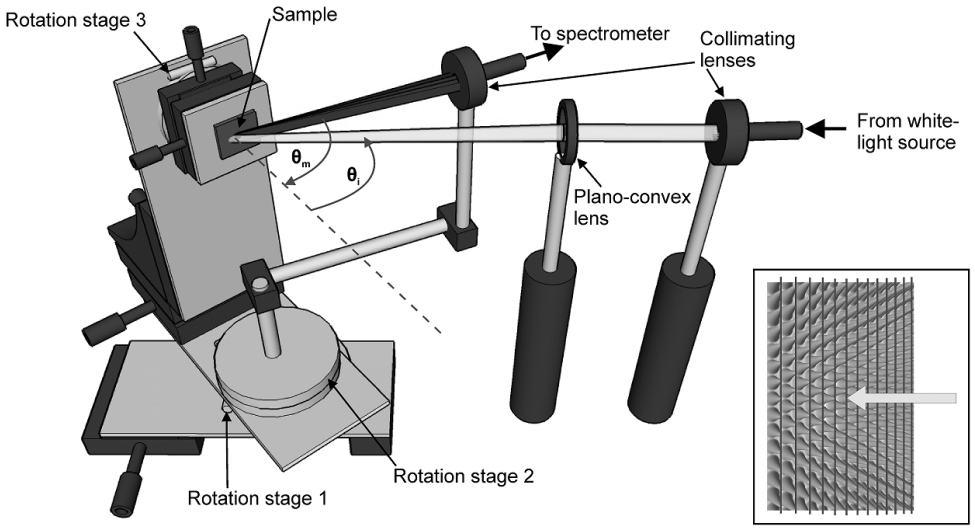

Fig. 6. Apparatus for characterizing silicon moth-eye samples. Inset shows orientation of moth-eye array with respect to incident light beam.

5. Results and discussion

Beginning with the single orientation sample, the variation in intensity of light with azimuth angle, at λ = 418 nm, collected at a fixed θ_i and θ_m, is presented in Fig. 7(ai). The angle of incidence was set to 85° and the angle of detection was 70° from the surface normal, producing the −1 diffraction order at λ = 418nm when nearest neighbour pillar planes are

#172279 - $15.00 USD Received 12 Jul 2012; accepted 15 Sep 2012; published 2 Jan 2013

aligned perpendicular to the incident beam, as predicted by the theory in Section 2.1. Six peaks were observed as the azimuth angle was rotated through 360°. These six peaks correspond to the symmetry of the hexagonal pattern and to the peaks in Fourier spectrum in Fig. 5(ci). The peak intensities show some variation with respect to each other and this is assigned to imperfections in optical alignment and inhomogeneities in the fabricated structures.

If the azimuth angle is fixed at one of the six peaks, the collector arm can be rotated to look at the spectral spread of the −1 diffractive order. The results of this for four different angles of incidence are presented in Fig. 7(b), along with the predicted results from the grating equation (Eq. (1)). The measurements match well to theoretical predictions, confirming the origin of the observed light as the −1 diffraction order.

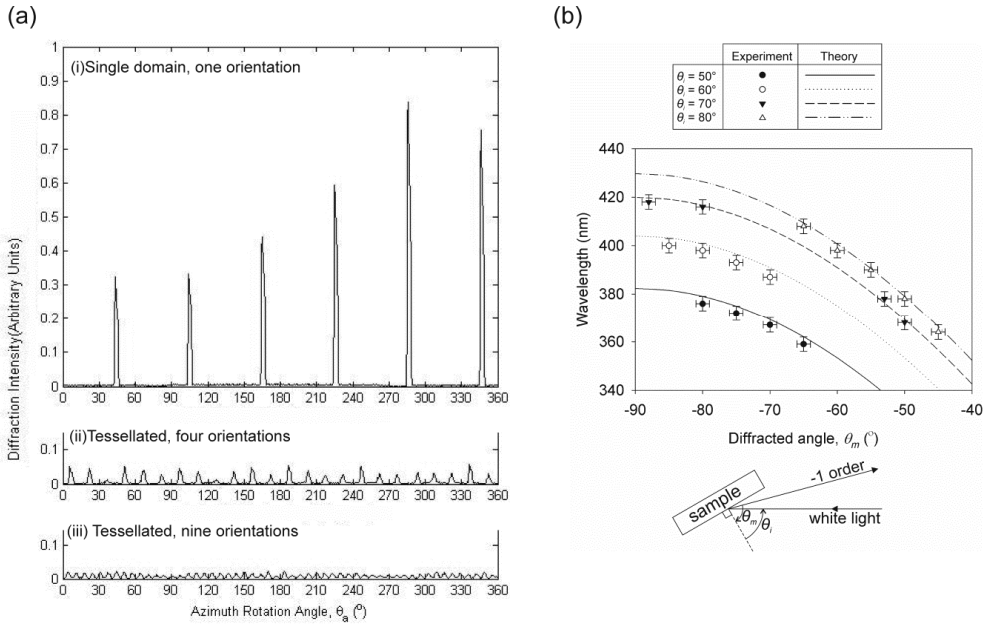

Fig. 7. (a) The variation of the intensity of the light of λ = 418 nm with azimuth angle, for a hexagonal moth-eye array of (i) single orientation, (ii) 4 orientations (tiled domains) and (iii) 9 orientations (tiled domains). The samples were illuminated with white light and θi and θm were fixed to collect the −1 diffracted order at λ = 418 nm (b) Plot showing the angle and wavelength of −1 diffraction orders produced using white light to illuminate a hexagonally arranged moth-eye array in silicon, with an inter-pillar spacing of 250 nm, at various angles of incidence. The lines show the theoretical results based on the one-dimensional grating equation. The points mark the measurements made with the apparatus in Fig. 6.

The same azimuth rotation experiment was performed on the two tiled samples. Again, the angle of incidence was 85° and the angle of detection 70°, with the 418nm wavelength peak monitored through an azimuth rotation of 360°. For the tiled samples consisting of domains with 4 and 9 orientations, 24 and 54 diffraction peaks were detected respectively (Fig. 7(a)(ii) and (iii)), matching the number of peaks in the Fourier spectra for these two patterns (Fig. 5(c)(ii) and (iii)). Furthermore, the intensity of each peak reduces as the number of orientations increases as there is less overall area of pattern contributing to each diffractive peak. The intensity of each diffraction peak in the 9 orientation tiled sample is only approximately 4.5% that of peaks for the single orientation sample.

The experiments show that artificial moth-eye surfaces for which the features are arranged in a regular array over a large area exhibit striking iridescence due to the emergence of the −1 diffractive order under specific illumination and viewing conditions. Furthermore, this effect can be greatly reduced by dividing up the array into domains of different orientations. This

#172279 - $15.00 USD Received 12 Jul 2012; accepted 15 Sep 2012; published 2 Jan 2013

increases the number of instances of the −1 diffractive order over a 360° azimuth rotation whilst reducing the intensity of each instance. If many orientations are included, then the −1 diffractive order is smeared out over the azimuthal space and its intensity at any one angle of azimuth is low. This explains why natural moth-eye arrays, whose features are arranged in disordered tessellated domains of hexagonally packed pillars, do not display noticeable iridescence. Whether this is an accident of the development mechanism employed or whether it is a genetically optimized stealth property has yet to be determined. It is clear however, that arrangement into domains reduces iridescence and so enhances inconspicuousness, reducing the likelihood of the insect being spotted by a predator. This approach also has implications for artificial moth-eye surfaces in technological applications. Iridescence caused by strong diffraction at certain angles would be undesirable for anti-glare screens on laptops, mobile phones and dashboards to which a moth-eye surface has been applied for antireflection. By designing the arrays in domains at various orientations, this effect could be avoided. Likewise, AR surfaces for lenses in stealth applications would be ineffective if at certain angles, the −1 diffractive order appeared, betraying the location of the piece of equipment designed to stay hidden. Employing a tiled pattern of domains for the antireflective array design would negate this.

The tiled patterns in this study were created in regular square-shaped domains in order to enable the specification of a repeatable unit cell which greatly simplifies the specification of the design on the e-beam lithography equipment used. However, this introduces a larger scale, domain-to-domain periodicity due to the periodic boundaries involved, and with that comes the possibility of other diffraction orders emerging depending on wavelength and domain size. The optimization of the domain size of regularly tiled domains is outside the scope of the current work but it is conceived to be important for the implementation of this approach from a practical viewpoint. In natural moth-eye arrays there is a degree of randomness inherent in the size and shape of the domains. Randomizing the size and shape of the domains so that they more closely resemble their natural counterparts would aid in removing regular periodic domain edges from the design thus greatly reducing unwanted diffraction. Such randomness is difficult to achieve over large areas in a pattern for e-beam lithography but it is conceivable that larger unit cells with a higher degree of randomness in the specification of domains could be defined in CAD software to minimize domain-to-domain diffraction. An example of such a pattern is shown in Fig. 8(a). Other strictly non-periodic patterns such as the ‘sunflower’ and ‘pinwheel’ patterns (Fig. 8(b) and 8(c)) [30,31], could be used to circumvent the problem of diffraction due to periodic domains. However, these patterns would require the specification of the position of each feature over a large area. Handling such large amounts of data would be a challenge for most e-beam lithography systems.

E-beam lithography is prohibitively expensive for the large area coverage demanded by most of the applications of artificial moth-eyes. Interference lithography, which involves exposing resist using the interference pattern created with intercepting coherent laser beams can be used to pattern areas on the tens of centimetre scale [32] but is inherently limited to defining regular patterns and so cannot be used for implementation of tiled domains or other symmetry-breaking designs. However, nanoimprint lithography [27] is not limited in this way and provides a possible route for large scale implementation of the patterns discussed in this work. Additionally, large scale self-assembly patterning techniques such as nanosphere lithography [33] could be used for cheap fabrication of such patterns [34,35], however control over specific domain size, shape and orientation using this technique is difficult. Nevertheless, methods of pre-patterning a surface to guide the self-assembly of nanospheres into the desired arrangements [36] could be investigated.

#172279 - $15.00 USD Received 12 Jul 2012; accepted 15 Sep 2012; published 2 Jan 2013

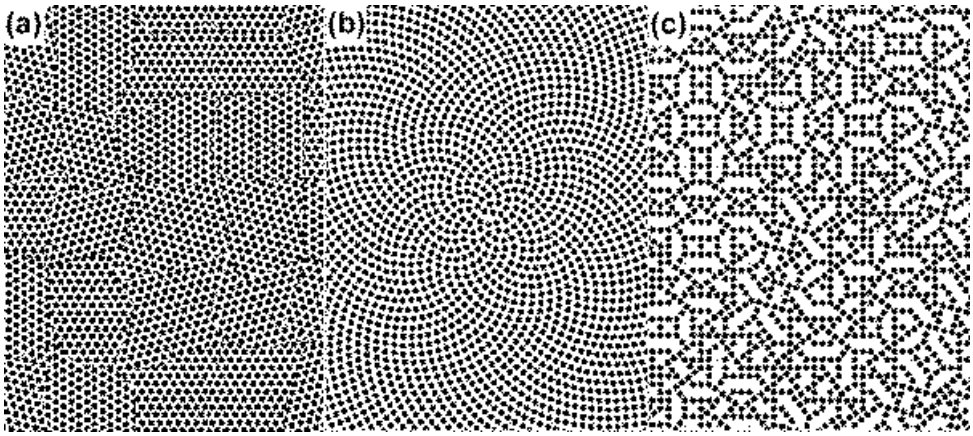

Fig. 8. Alternative patterns for reducing diffraction caused by domain-to-domain periodicity: (a) increased randomness in the size and shape of domains within a unit cell; (b) 'sunflower' pattern; (c) Conway 'pinwheel' pattern.

6. Conclusion

In this work, the diffraction emerging from sub-wavelength arrays of silicon pillars with a period of 250nm at large angles of incidence has been investigated. Taking inspiration from the arrangement of features in natural moth-eyes, a new tiled-domain design was implemented. It was demonstrated the division of the array into domains with different orientations of the hexagonal close-packed structure breaks the symmetry of the array and so reduces the intensity of the minus 1 diffraction order noticed at high angles of incidence. This implies that natural moth-eyes may have evolved tiled domain arrays due to their useful combination of low diffraction intensity and efficient antireflection properties which would allow them to simultaneously see more efficiently in low lighting conditions whilst also avoiding predators. Intense diffraction orders would introduce iridescence, thus destroying the camouflaging effect and making them vulnerable to detection under certain illumination conditions. Such a tiled-domain array could be used as a more practical solution to creating low-diffraction sub-wavelength surfaces compared to complex symmetry-breaking designs based on quasi-crystal-type aperiodic tiling and Fibonacci/'Sunflower' spirals. It could also be envisaged that this type of solution can be useful for the design of artificial moth-eye surfaces for antiglare and stealth applications where both high antireflection performance and low diffraction is required.

#172279 - $15.00 USD Received 12 Jul 2012; accepted 15 Sep 2012; published 2 Jan 2013